Fermi National Accelerator Laboratory

FERMILAB-Conf-94/088-E

CDF

Electroweak and b-Physics at the Tevatron Collider

K. Hara

University of Tsukuba, Institute of Physics, Tsukuba-shi
Ibaraki-ken 305, Japan

Fermi National Accelerator Laboratory
P.O. Box 500, Batavia, Illinois 60510

April 1994

Presented at the *INS Symposium*, Tokyo, Japan, March 8-10, 1994

Operated by Universities Research Association Inc. under Contract No. DE-AC02-76CHO3000 with the United States Department of Energy

FERMILAB-CONF-94/088-E

CDF/PUB/ELECTROWEAK/PUBLIC/2534
DØ note #2100
22 INS symposium, Tokyo, 8-10 March 1994

Electroweak and b-Physics at the Tevatron Collider

K. Hara
University of Tsukuba/CDF
Institute of Physics, Tsukuba-shi, Ibaraki-ken 305, Japan

Abstract: The CDF and DØ experiments have collected integrated luminosities of 21 pb^{-1} and 16 pb^{-1}, respectively, in the 1992–1993 run (Run Ia) at the Fermilab Tevatron. Preliminary results on electroweak physics are reported from both experiments: the W mass, the leptonic branching ratios $\Gamma(W \to \ell\nu)$, the total W width, gauge boson couplings, W decay asymmetry and W'/Z' search. Preliminary new results on b physics are presented: B^0-$\overline{B}^0$ mixing from DØ, and masses and lifetimes of B-mesons from CDF.

1 Introduction

In the 1992–1993 data taking run (Run Ia), the two experiments CDF and DØ at the Fermilab Tevatron have collected integrated luminosities of approximately 21 pb^{-1} and 16 pb^{-1}, respectively, at $\sqrt{s} = 1.8$ TeV. Run Ia is the first data taking run for DØ. CDF has been upgraded by addition of silicon vertex detector (SVX) and a second set of muon chambers. The preliminary CDF results presented here use the full data sample. The DØ results are also preliminary, and the analyses of some of the subjects are based on a part of the accumulated data, 8 pb^{-1} for the muon data sample and 16 pb^{-1} for the electron data sample. The CDF detector[1] and DØ detector[2] are described elsewhere.

The subjects covered and availability of analysis results are summarized below: — denotes the result is not available. Since only the muon charge is measurable by the DØ detector, they report W decay asymmetry and B^0-$\overline{B}^0$ mixing in the muon channel. CDF collected an integrated luminosity of $\sim$4 pb^{-1} in the 1988–89 data taking run. These results, denoted by 88 in the table, have been published elsewhere.

Electroweak Physics	CDF	DØ
W mass	e,μ	e
$R = \sigma \cdot B_{W\to l\mu}/\sigma \cdot B_{Z\to ll}$	e,μ	e,μ
$W\gamma$	e,μ	e,μ
$Z\gamma$	e,μ	—
WZ	1 event	—
W decay asymmetry	e,μ	μ
W'/Z' search	$88(e+\mu)/e$	e/e

b Physics	CDF	DØ
B^0-$\overline{B}^0$ mixing	88 $(e+\mu)$	μ
B_u, B_d masses	exclusive J/ψ K	—
B_s mass	exclusive J/ψ ϕ	—
B_u, B_d lifetimes	exclusive J/ψ K	—
B_s lifetime	$D_s + l + X$	—

2 W mass measurement

Since a precise Z boson mass is available from the LEP experiments, the Standard Model can specify all the electroweak parameters, apart from the top quark mass and the Higgs sector. The best estimate to the W mass is 80.25±0.10 GeV/c^2[3]. Accurate W mass measurements at the Tevatron permit an overconstrained fit of the electroweak parameters and thus we can test the Model. In future, provided with an accurately known top mass, these measurements can give constraints on possible Higgs masses.

At the Tevatron collider, W's and Z's are produced predominantly through valence quark–antiquark annihilation. CDF and DØ identify W's by the subsequent leptonic decays, where one high p_T lepton (e or μ) and a large unbalanced E_T due to the escaping ν are detected. Z's are identified by decays into two high p_T leptons (e^+e^- or $\mu^+\mu^-$).

Table 1 summarizes the lepton selections for identification of W's and Z's. The selections are used for the R measurement described in the next section. CDF raised the ${E_T}^e$ and missing E_T cuts to 25 GeV and added jet rejection and p_T^W cuts for the W mass measurement. DØ does not quote a W mass in the muon channel, since the number is not competitive.

In order to extract the W mass, both experiments fit the MC generated distribution to the measured transverse mass distribution, $M_T = \sqrt{2E_T^\ell E_T^\nu(1 - cos\phi_{\ell\nu})}$, where $\phi_{\ell\nu}$ is the azimuthal angle between the lepton and neutrino. It is crucial that realistic $\vec{P}_W$ spectrum is available in the MC in order to reproduce the M_T distribution correctly. CDF models the $\vec{P}_W$ using a $\vec{P}_L^W$ calculated from structure functions and a $\vec{P}_T^W$ taken from the measured $\vec{P}_T^Z$ distribution with a scale factor multiplied. DØ uses a theoretical calculation[4] with minimum bias events overlaid.

The CDF μ momentum scale is determined by fitting the reconstructed masses of J/ψ and Υ resonances, and e energy scale from the calorimeter-energy-to-track-momentum (E/p) ratio. The DØ e scale is determined using the Z mass measured by the LEP experiments. In order to establish the neutrino E_T scale, the calorimeter response to the low energy hadrons recoiling against the W has to be fully understood. Both experiments use the Z events to study the systematics in the neutrino E_T measurement. Using the relation between $\vec{P}_T^Z$ and recoiling jet energy in the Z events, DØ corrects the neutrino E_T scale based on the difference of the two. CDF uses the measured calorimeter energy in the Z events with the same P_T^Z as the MC generated P_T^W. The scale factor multiplied to $\vec{P}_T^Z$ is determined by comparing the distributions of the recoil jets associated with W's and Z's.

The M_T distributions are shown in Fig. 1 for CDF $W \to \mu\nu$ and DØ $W \to e\nu$ events. The preliminary W mass measurements are summarized as (in GeV/c^2):

CDF $W \to e\nu$	$80.47 \pm 0.15(stat) \pm 0.19(syst) \pm 0.10(SF) \pm 0.13(scale)$
CDF $W \to \mu\nu$	$80.29 \pm 0.20(stat) \pm 0.19(syst) \pm 0.10(SF) \pm 0.06(scale)$
CDF $e + \mu$ combined	80.38 ± 0.23
DØ $W \to e\nu$	$79.86 \pm 0.16(stat) \pm 0.19(syst) \pm 0.07(SF) \pm 0.31(scale)$
CDF + DØ combined	80.25 ± 0.21

Table 1. Event selections for W and Z identification in the muon and electron decay channels. Cut values are for the R measurement. Pseudo-rapidity is defined as: $\eta = -\ln tan(\theta/2)$, where θ is the polar angle with respect to the proton direction. Separation in the (η, ϕ) plane is defined as: $\Delta R = \sqrt{\Delta\eta^2 + \Delta\phi^2}$.

	CDF	DØ
Primary e:		
E_T cut (coverage)	$E_T > 20$ GeV ($\|\eta\| < 1.1$)	$E_T > 25$ GeV ($\|\eta\| < 1.1$)
shower shape	lateral sharing < 0.2	lateral+longitudinal profile
	$\chi^2_{\rm SMD} < 10$ (SMD:shower max det)	$\chi^2 < 100$ for 41 dof
isolation	$E_T^{\Delta R<0.4}/E_T < 1.1$	$E^{\Delta R<0.4}/E^{\Delta R<0.2} < 1.15$
E/p match	$0.5 < E/p < 2.0$	
trk-calor match	$\delta x_{trk-SMD} < 1.5$ cm	$\delta x_{trk-clst} < 10\sigma_{clst}$
hadronic leakage	Had/EM $< 0.055 + 0.00045E$	EM/(EM+Had) > 0.9
event vertex	$\|z_{vtx}\| < 60$ cm	
Neutrino:		
missing E_T cut	$E_T > 20$ GeV	$E_T > 25$ GeV
Secondary e:		
p_T cut (coverage)	$E_T > 20$ GeV ($\|\eta\| < 1.1$)	same as Primary
	$E_T > 15$ GeV ($1 < \|\eta\| < 2$)	
	$E_T > 10$ GeV ($2 < \|\eta\| < 4$)	
isolation	same as Primary	same as Primary
hadronic leakage	Had/EM < 0.1	same as Primary
other cuts		same as Primary
energy scale	E/p ratio	Z ($M_Z = 91.187$ GeV/c^2)
		(J/ψ , π^0 under study)
Primary μ:		
p_T cut (coverage)	$p_T > 20$ GeV/c ($\|\eta\| < 0.63$)	$p_T > 20$ GeV/c ($\|\eta\| < 1.7$)
calorimeter energy	Had < 6; EM < 2 GeV	Had+EM $> 0.5^{\rm in\,cc}$,$> 1^{\rm in\,fc}$ GeV
isolation	$E_T^{\Delta R<0.4} < 2$ GeV	$-2\sigma_{mip} < E_{0.2\times0.2} < 3\sigma_{mip}$
μ-central track match	$\delta x_{\rm inner(outer)} < 2(5)$ cm	$\Delta\phi < 0.35$ rad; $\Delta\theta < 0.45$ rad
attach to event vertex	< 5 cm with $\|z_{evt}\| < 60$ cm	< 25 cm$^{\rm in\,3D}$, < 10 cm$^{\rm in}\phi$
Neutrino:		
missing E_T cut	$E_T > 20$ GeV	$E_T > 20$ GeV
Secondary μ:		
p_T cut (coverage)	$p_T > 20$ GeV/c ($\|\eta\| < 1.2$)	$p_T > 15$ GeV/c ($\|\eta\| < 1.7$)
calorimeter energy	Had < 6; EM < 2 GeV	
attach to event vertex	< 5 cm with $\|z_{evt}\| < 60$ cm	
$\mu\mu$ angles		$30° < \phi_{\mu\mu} < 160°$;$\theta_{\mu\mu} < 170°$
other cuts	cosmic ray filter	cosmic ray filter
momentum scale	J/ψ, Υ's; Z as a check	field map+alignment
		(Z,J/ψ under study)

The main contributors in the systematics are the energy resolution (0.14/0.12 GeV/c^2 for CDF e/μ, and 0.15 GeV/c^2 for DØ), $\vec{P}_T^W$ modelling (0.11/0.14 GeV/c^2 for CDF e/μ,

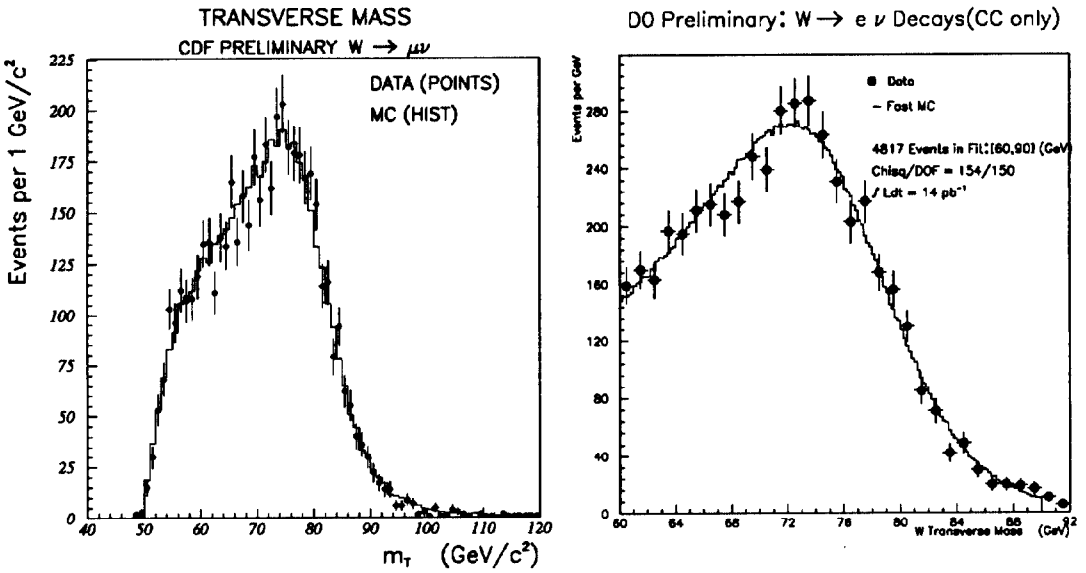

Figure 1: Transverse mass distributions for (left) CDF $W \to \mu\nu$ and (right) DØ $W \to e\nu$ events.

0.05 GeV/c^2 for DØ). Uncertainties due to the structure function (SF) and energy scale are quoted separately.

Since the M_T distribution of background events, such as $W \to \tau\nu, Z \to ee/\tau\tau$ and QCD backgrounds (in $W \to e\nu$ channel), are different, CDF and DØ have studied in detail the W mass shift due to the backgrounds. CDF includes a correction of +0.11 (+0.23) GeV/c^2 in the W mass in the e (μ) decay channel.

3 R measurement

The ratio of the W and Z cross sections in the e and μ decay channels, R_ℓ, is a good quantity at the Tevatron collider to measure the leptonic decay branching ratios and the W total width Γ_W. The branching ratio is sensitive to unknown decay modes of the W, which can place a model independent limit on the mass of the top quark. The leptonic decay widths to electron and muon can test lepton universality using real W's.

The ratio R_ℓ can be expressed as:

$$R_\ell = \frac{\sigma B(W \to \ell\nu)}{\sigma B(Z \to \ell\ell)} = \frac{\sigma_W \cdot \Gamma(W \to \ell\nu)/\Gamma_W}{\sigma_Z \cdot \Gamma(Z \to \ell\ell)/\Gamma_Z}. \quad (1)$$

$\Gamma(W \to \ell\nu)$ and Γ_W are extracted from R by using the following numbers from theories and LEP experiments:

	CDF	DØ
σ_W/σ_Z	3.33 ± 0.03[5]	3.26 ± 0.08[6]
$\Gamma(W \to \ell\nu)/\Gamma(Z \to \ell\ell)$	2.696 ± 0.018[7]	2.696 ± 0.018[7]
Γ_Z in GeV	2.489 ± 0.007[8]	2.487 ± 0.010[9]
$\Gamma(Z \to ee)$ in MeV	83.33 ± 0.30[8]	83.24 ± 0.42[9]
$\Gamma(Z \to \mu\mu)$ in MeV	83.78 ± 0.40[8]	83.24 ± 0.42[9]

The advantage of taking the ratio is that many uncertainties in the cross section measurements cancel or are reduced, such as the integrated luminosity, common terms in W and Z detection efficiencies, and the systematic uncertainties in the W and Z acceptances.

DØ reports the W and Z cross sections. The cross sections, the R value, the W total width are summarized in Table 2. The new DØ cross section measurements can be compared with the published data by CDF[10]. The W and Z cross sections by CDF and DØ agree with each other, and they, together with UA1 and UA2 measurements, are described well by theoretical calculations, for example, by Ref [11].

Table 2. Cross sections for W and Z productions, R_ℓ, and W total decay width Γ_W^ℓ measured in the e and μ decay channels. The numbers are preliminary except for the cross sections from CDF[10]. First errors are statistical, second systematic. Uncertainty in the luminosity is separately shown for the cross sections.

	CDF	DØ
$\sigma B(W \to e\nu)$ (nb)	$2.19 \pm 0.04 \pm 0.14 \pm 0.15$ (lum)	$2.25 \pm 0.03 \pm 0.10 \pm 0.27$ (lum)
$\sigma B(W \to \mu\nu)$ (nb)	$2.21 \pm 0.07 \pm 0.14 \pm 0.15$ (lum)	$2.00 \pm 0.07 \pm 0.41 \pm 0.24$ (lum)
$\sigma B(Z \to ee)$ (nb)	$.209 \pm .013 \pm .009 \pm .014$ (lum)	$0.21 \pm 0.01 \pm 0.01 \pm 0.02$ (lum)
$\sigma B(Z \to \mu\mu)$ (nb)	$.226 \pm .022 \pm .018 \pm .014$ (lum)	$0.20 \pm 0.02 \pm 0.05 \pm 0.02$ (lum)
R_e	$10.86 \pm 0.32 \pm 0.28$	$10.70 \pm 0.60 \pm 0.50$
R_μ	$12.38 \pm 0.63 \pm 0.45$	$10.0 \pm 1.1 \pm 2.4$
Γ_W^e (GeV)	$2.07 \pm 0.06 \pm 0.06$	$2.05 \pm 0.11 \pm 0.11$
Γ_W^μ (GeV)	$1.80 \pm 0.11 \pm 0.09$	$2.19 \pm 0.24 \pm 0.53$

The W total width, a fundamental constant of the Model, agrees excellently with the Standard Model prediction 2.067 ± 0.021 GeV[7].

The measurement of the branching ratio is sensitive to new decay modes of the W. One such decay mode would be W decaying to top. The measurement provides a limit on the top quark mass independent of the presumed top decay channels in the mass region $M_{top} < M_W - M_b$, since the W can decay into a real top and contribute to the W width. The predicted value of the branching ratio is plotted in Fig. 2 as a function of the top mass. We use this ratio since it depends weakly on the W mass. The CDF and DØ R_e values and 95% upper limits are also shown. The corresponding top mass limit is 62 GeV/c^2 by CDF[12] and 56 GeV/c^2 by DØ at 95% CL.

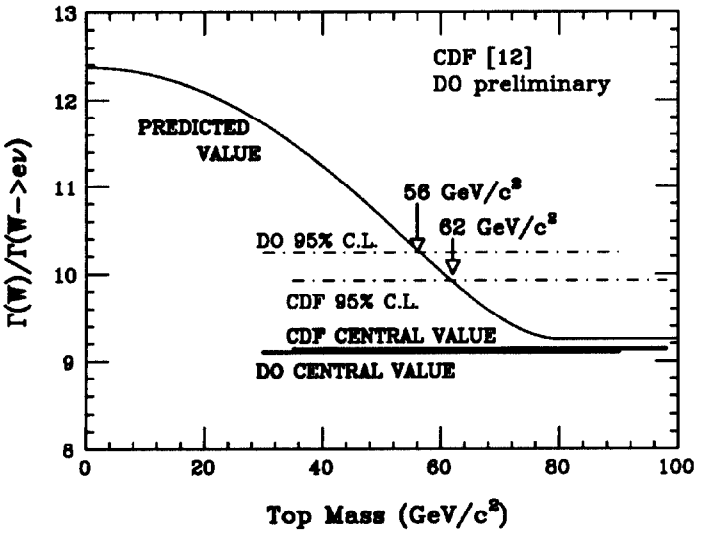

Figure 2: The predicted value for $\Gamma(W)/\Gamma(W \to e\nu)$ from the Standard Model, and CDF and DØ measurements. Dot-dashed lines are 95% CL upper limits.

4 $W\gamma$ coupling

Measurement of gauge boson couplings is now becoming feasible at the Tevatron, as we collect large statistics samples of W and Z bosons. Among the various gauge boson combinations, the channel involving $W\gamma$ is expected to have the largest cross section. The trilinear coupling of the gauge bosons is completely specified in the Standard Model. Anomalous couplings can be non-zero in some extensions such as in composite models, and, if they exist, will modify the event rates and distributions.

The lowest order $W\gamma$ production diagrams are shown in Fig. 3 (V=W). The most general, gauge and Lorentz invariant effective Lagrangian[13] is expressed as:

$$\begin{aligned} L_{WW\gamma} &= -ie[(W^\dagger_{\mu\nu}W^\mu A^\nu - (W^\dagger_\mu A_\nu W^{\mu\nu}) + \kappa W^\dagger_\mu W_\nu F^{\mu\nu} + \frac{\lambda}{M_W^2} W^\dagger_{\sigma\mu} W^\mu_\nu F^{\nu\sigma} \\ &\quad + \kappa' W^\dagger_\mu W_\nu \tilde{F}^{\mu\nu} + \frac{\lambda'}{M_W^2} W^\dagger_{\sigma\mu} W^\mu_\nu \tilde{F}^{\nu\sigma} \end{aligned} \tag{2}$$

where $W_{\mu\nu} = \partial_\mu W_\nu - \partial_\nu W_\mu$, $F_{\mu\nu} = \partial_\mu A_\nu - \partial_\nu A_\mu$, and $\tilde{F}_{\mu\nu} = \frac{1}{2}\epsilon_{\mu\nu\sigma\rho}F^{\sigma\rho}$. This Lagrangian gives rise to electromagnetic moments of W^+:

magnetic dipole	$\mu_W = \frac{e}{2M_W}(1+\kappa+\lambda)$	$\to \frac{e}{M_W}$
electric quadrupole	$Q_W = -\frac{e}{M_W^2}(\kappa-\lambda)$	$\to -\frac{e}{M_W^2}$
electric dipole	$d_W = \frac{e}{2M_W}(\kappa'+\lambda')$	$\to 0$
magnetic quadrupole	$Q'_W = -\frac{e}{M_W^2}(\kappa'-\lambda')$	$\to 0$

In the Standard Model, $\Delta\kappa \equiv 1-\kappa = \lambda = \kappa' = \lambda' = 0$, these moments are reduced to the values listed in the last column. Among the above anomalous couplings, $\Delta\kappa$ and λ are CP conserving terms, and κ' and λ' are CP non-conserving.

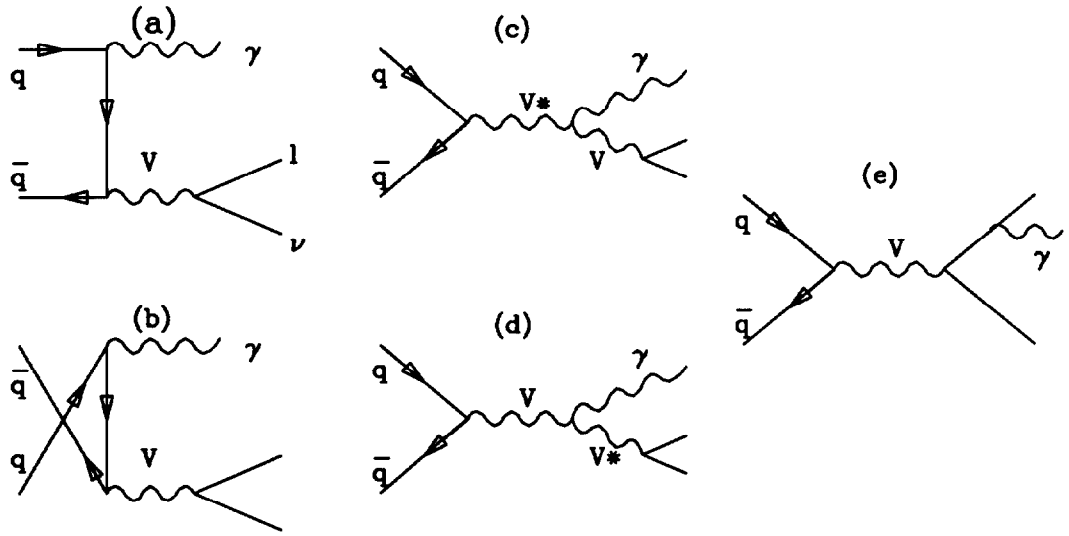

Figure 3: Lowest order diagrams of $V+\gamma$ production: (a) u-channel, (b) t-channel, (c) s-channel (V "production"), (d) s-channel ("radiative" V decay), (e) internal bremsstrahlung.

The photons are identified by requiring an EM cluster with no track pointing to it. The γ coverage in $|\eta|$ is 1.1 by CDF and 3.2 by DØ, and the E_T cut is 7 GeV by CDF and 10 GeV by DØ. Both groups require a tighter requirement for the isolation cut than that for electrons, and the separation between the γ and the lepton (e or μ) from W decay to be $\Delta R_{\ell\gamma} > 0.7$ to suppress internal bremsstrahlungs (the diagram (e) of Fig. 3), and to allow precise energy reconstruction of both the γ and the lepton. CDF uses extensively the Shower Max Detector (SMD) implemented in the EM calorimeter to reject π^0/η's, which are the main source of the background.

Table 3. Summary of the $W\gamma$ events and the limits on the anomalous couplings (preliminary).

	CDF	DØ
$W\gamma$; $W \to e\nu$		
No of signal events	$13.6 \pm 4.5 \pm 3.5$	$6.1 \pm 4.2 \pm 1.8$
No of backgrounds	$5.4 \pm 1.1 \pm 1.5$	3.9 ± 1.8
No of expected (SM)	$17.0 \pm 1.8 \pm 2.3$	$8.7 \pm 0.9 \pm 1.1(lum)$
$W\gamma$; $W \to \mu\nu$		
No of signal events	$3.7 \pm 2.6 \pm 0.6$	$6.0 \pm 4.2^{+1.0}_{-0.5}$
No of backgrounds	$0.4 \pm 0.1 \pm 0.2$	$4.0^{+1.0}_{-0.5}$
No of expected (SM)	$8.6 \pm 0.9 \pm 1.7$	$6.9 \pm 1.0 \pm 0.8(lum)$
$e+\mu$ combined limits (95% CL)		
$(\lambda = 0)$	$-2.3 < \Delta\kappa < 2.2$	$-2.5 < \Delta\kappa < 2.7$
$(\Delta\kappa = 0)$	$-0.7 < \lambda < 0.7$	$-1.2 < \lambda < 1.1$
$(\lambda' = 0)$	$-2.3 < \Delta\kappa' < 2.2$	
$(\Delta\kappa' = 0)$	$-0.7 < \lambda' < 0.7$	

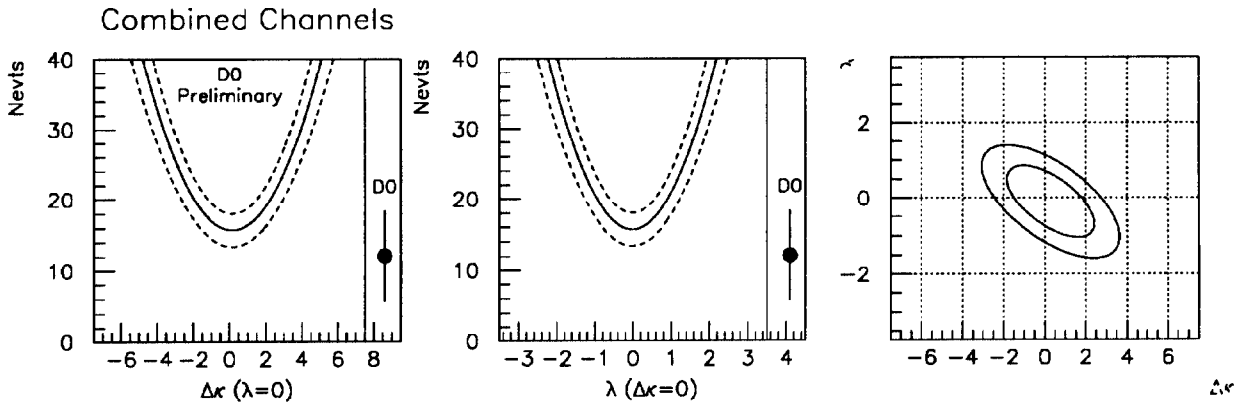

Figure 4: Limits on anomalous $W\gamma$ couplings (DØ preliminary). The contours show the limits at 68% and 95% CL.

The preliminary $W\gamma$ event rate, background rate and the Standard Model prediction are summarized in Table 3. Also listed in the table is the 95% CL limits on anomalies. The main background is W+jets events with one of the jets misidentified as a photon. Both groups have studied the probability that a QCD jet passes the photon identification cut, and multiplied it to the number of W+jets events to evaluate this background rate. Other backgrounds considered are $Z + \gamma$/jets events with one of the Z decay leptons being missed by the detector, $W\gamma$ with $W \to \tau\nu$, and Drell-Yan + γ/jets.

DØ has extracted the limits from the $W\gamma$ event rate. The e and μ combined event rate is compared in Fig. 4 with the expectations as a function of the anomalous coupling $\Delta\kappa$ (λ) with λ ($\Delta\kappa$) fixed to zero. The limits are expressed in the $\lambda - \Delta\kappa$ plane as shown in the

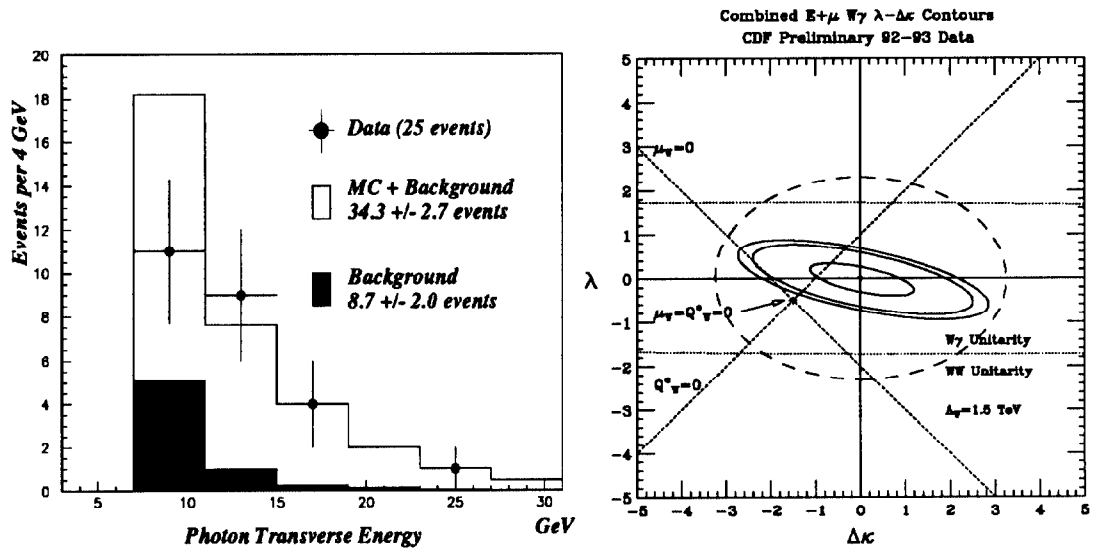

Figure 5: E_T^γ distribution is compared with Standard Model prediction (CDF preliminary). From the distribution, CDF extracts the limits as shown in the contours: three contours correspond to the limits at 68%, 90% and 95% CL.

figure. These new measurements improve substantially the previous measurements done by UA2[14].

CDF has calculated the limits from the shape of the E_T^γ distribution. The diagrams (a)-(d) in Fig. 3 interfere destructively ("radiation-zero" or gauge cancellation) in the Standard Model. Presence of anomalous couplings implies the lack of full gauge cancellation and results in higher event rate. Enhancement of the $W\gamma$ cross section is pronounced in the tail of the E_T^γ distribution. The e and μ combined E_T^γ distribution and the Standard Model prediction are compared in Fig. 5. The distribution is well described by the Standard Model prediction. The limits on CP-conserving anomalous couplings are shown in the figure.

The two dotted lines in the figure cross at a point where the W magnetic-dipole and electric-quadrupole moments are zero, which is excluded by the present measurement. Also CDF concludes that at 90% CL the magnetic-dipole moment of W^+ is positive.

5 $Z\gamma$ coupling

The processes for $Z\gamma$ production are similar to $W\gamma$ shown in Fig. 3 ($V = Z$ and ν reads charged lepton), except that diagrams (c) and (d) do not exist in the Standard Model. Because the destructive interference is not present, the $Z\gamma$ rate is almost comparable to the $W\gamma$ rate ($\sigma B_{Z\gamma}/\sigma B_{W\gamma} \sim \frac{1}{4}$ compared to $\sigma B_Z/\sigma B_W \sim \frac{1}{10}$).

The most general gauge and Lorentz invariant anomalous $ZZ\gamma$ vertex is:[15]

$$\Gamma_{Z\gamma Z}^{\alpha\beta\mu}(q_1, q_2, P) = \frac{P^2-q_1^2}{M_Z^2} \times [h_1^Z(q_2^\mu g^{\alpha\beta} - q_2^\alpha g^{\mu\beta}) + \frac{h_2^Z}{M_Z^2} P^\alpha (P \cdot q_2 g^{\mu\beta} - q_2^\mu P^\beta) + h_3^Z \epsilon^{\mu\alpha\beta\rho} q_{2\rho} + \frac{h_4^Z}{M_Z^2} P^\alpha \epsilon^{\mu\beta\rho\sigma} P_\rho q_{2\sigma}] \quad (3)$$

where P and q_1 are the incoming and outgoing Z boson four-momenta, and q_2 is of the outgoing γ. The $Z\gamma$ final state includes the processes where the intermediate Z in (c) and (d) in Fig. 3 is replaced with γ^*. The $Z\gamma\gamma$ vertex can be defined similarly. Since all the anomalous terms violate unitarity, CDF assumes that h_i's are expressed in form factors and are constrained by unitarity:[16]

$$h_i^V(P^2 = \hat{s}, q_1^2 = M_Z^2, q_2^2 = 0) = \frac{h_{i0}^V}{(1 + \hat{s}/\Lambda^2)^n}. \quad (4)$$

CDF places the limits on h_{i0}^V with assuming $n = 3$ for $i = 1, 3$, $n = 4$ for $i = 2, 4$, and $\Lambda = 0.5$ TeV.[17]

Table 4. Limits on anomalous $ZZ\gamma$ and $\gamma\gamma Z$ couplings at 95% CL obtained by CDF (preliminary).

$ZZ\gamma$ vertex	$\gamma Z\gamma$ vertex
$-2.9 < h_{10}^Z < 3.0$	$-3.1 < h_{10}^\gamma < 3.1$
$-0.7 < h_{20}^Z < 0.7$	$-0.8 < h_{20}^\gamma < 0.8$
$-2.9 < h_{30}^Z < 3.0$	$-3.1 < h_{30}^\gamma < 3.1$
$-0.7 < h_{40}^Z < 0.7$	$-0.8 < h_{40}^\gamma < 0.8$

Among these couplings, h_{30} and h_{40} are CP conserving and h_{10} and h_{20} are non-conserving terms. The transition moments of the Z boson are related to these quantities through, for example, transition magnetic dipole moment $g_{Z_T} = \sqrt{2}(h_{10}^Z - h_{20}^Z)$.

6 WW and WZ coupling

Trilinear gauge couplings can be probed also by measuring $W + Z$ production and $W + W$ production. The Standard Model cross sections in $p\bar{p}$ collisions at 1.8 TeV are 9.5 pb for $W+W$, 2.5 pb for $W+Z$ and 1.0 pb for $Z+Z$ production. The tri-lepton signature in $W+Z$ channel is distinctive and has the least background among the all diboson decay channels, but is suppressed significantly by the leptonic branching ratios.

CDF has seen one $W + Z$ candidate in 21 pb^{-1}, where W and Z decay into the electron modes. One dielectron pair reconstructs to an invariant mass of $\sim$82 GeV/c^2, consistent with Z, and the third electron and the missing E_T reconstruct to a transverse mass of $\sim$75 GeV/c^2, consistent with W.

Two missing neutrinos are involved in the leptonic decay in the $W + W$ channel, which makes event reconstruction complicated. Since this channel is an important source of the background for top search, detailed studies are being carried out.

Analysis is in progress to extend the search into (partially) hadronic decay modes to increase the event rate at a cost of increased background.

7 W decay asymmetry

Primarily, W^+ (W^-) bosons are produced in $p\bar{p}$ collisions by the annihilation of u (d) quarks from the proton and $\bar{d}$ ($\bar{u}$) quarks from the antiproton. Since the u ($\bar{u}$) quark tends to carry a larger fraction of the hadron momentum than the d ($\bar{d}$) quark, the W^+ (W^-) tends to be boosted in the proton (antiproton) direction. The forward-backward asymmetry of the charged leptons from W decay occurs through the combination of the difference in u and d distributions in the initial hadrons and the $(V - A)$ character of the subsequent charged current decay. Since the $(V - A)$ character is well measured by muon decay experiments, the W decay asymmetry can probe the quark structure of the proton.

The asymmetry is defined as:

$$A(\eta) = \frac{d\sigma^+/d\eta - d\sigma^-/d\eta}{d\sigma^+/d\eta + d\sigma^-/d\eta}, \tag{5}$$

where η is the pseudo-rapidity of the decay lepton. Because of CP invariance, the asymmetry in positive η is equal in magnitude and opposite in sign to that in negative η. This property can be used to combine the values at negative and positive η together, which reduces the effect of any differences in the efficiencies for positive and negative leptons.

CDF has measured the asymmetry in $W \to e\nu$ and $W \to \mu\nu$ channels, and the data are combined. The asymmetry data is plotted in Fig. 6 together with predictions using various structure functions. The CDF data is sensitive to exclude some of the structure functions: The data favors MRS D$_-$ and MRS D$_0$, and disfavors MTB1 and KMRS B$_0$ structure functions. The W asymmetry data is particularly sensitive to the slope of the d/u

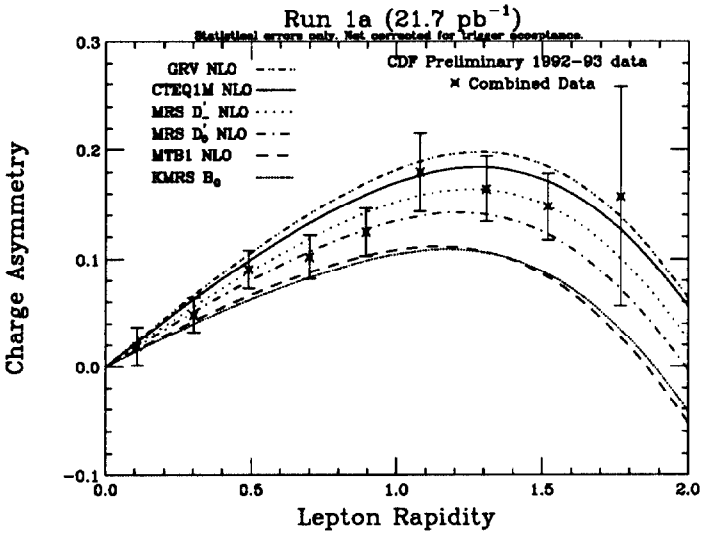

Figure 6: The charge asymmetry of leptons from W decay (CDF preliminary). Predictions using various structure functions are overlaid.

ratio versus x[16] at high Q^2 ($\sim M_W^2$), whereas the $F_2^{\mu n}/F_2^{\mu p}$ measurements are sensitive to the magnitude of the ratio. Since the errors in the asymmetry data are still dominated by the statistical errors, more accurate measurement can be made in near future.

DØ has measured the asymmetry in muon decay mode with the toroidal magnet polarity reversed for certain periods to reduce the systematic effect associated in the charge determination. Although the asymmetry data agrees in general with the CDF data, DØ data can so far not distinguish various structure functions because of the fairly large errors on the data points.

8 W' and Z' search

Many extensions to the Standard Model predict the existence of additional gauge bosons W' and Z'. Extensions include such models as E_6, which could specify the coupling strengths to quarks and leptons but make no prediction for the additional gauge boson masses.

The mass limits on W' and Z' have been so far set by the CDF group obtained using the 88-89 data[19]. The searches were made in combined electron and muon decay channels. CDF has extended the search in $Z' \rightarrow ee$ mode using the new data. DØ reports the searches for W' and Z' in electron channels.

Searches look for the excess in the high mass tail in the dilepton invariant mass distribution for Z' and the transverse mass distribution for W'. The searches are summarized in Fig. 7. CDF compares the $\sigma \cdot B$ seen and that expected as a function of M_{ee}. The Z' couplings to quarks and leptons are assumed to be identical to ordinary Z, and the Z' width is set to be proportional to the mass. The limit on the Z' mass is 495 GeV/c^2 at 95% CL.

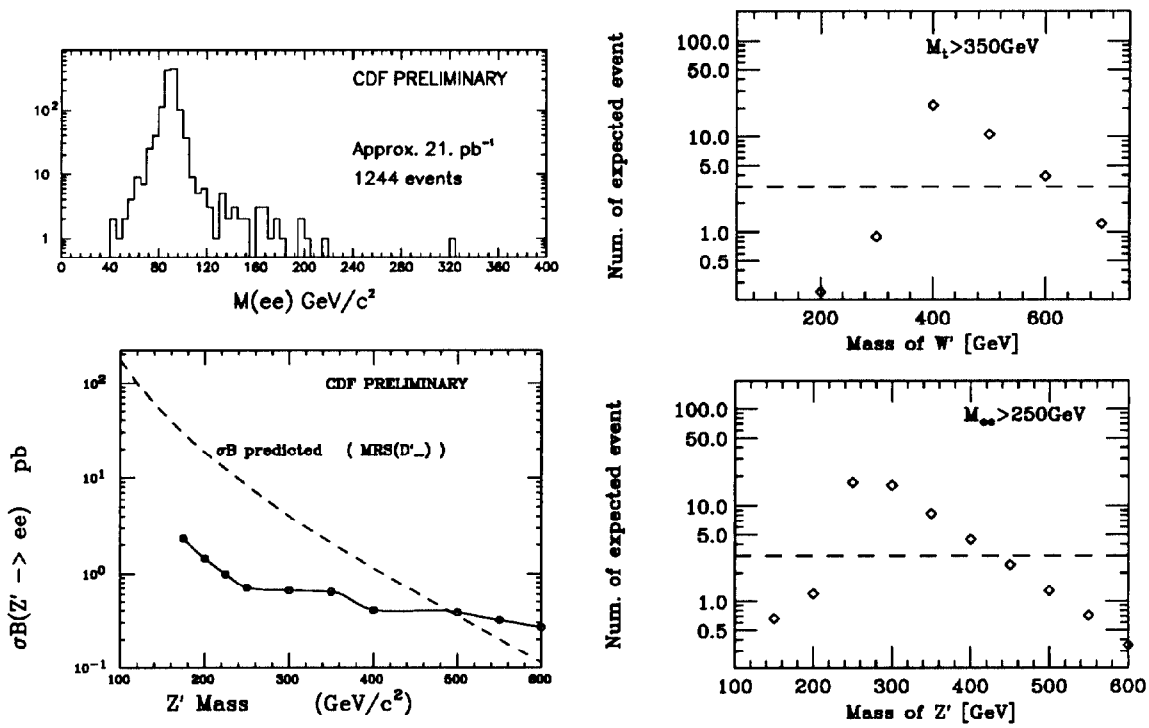

Figure 7: Left: Dielectron invariant mass distribution measured by CDF, and upper limit of the cross section at 95% CL in comparison with prediction for Z' production. Right: Upper limit (95% CL) of the number of events observed by DØ (line) in comparison with the number expected for W' and Z' productions (diamonds).

Note that one event seen $\sim$320 GeV/c^2 is in agreement with the Drell-Yan expectations. CDF has extracted the lower mass limits for four different Z' models from the E_6 symmetry group. The details can be found elsewhere[20]. The published CDF limit on W' mass is 520 GeV/c^2 at 95% CL.

DØ compares the number of events seen and of expected above certain masses. In order to be sensitive to high mass and low mass W' and Z', M_T cuts are chosen at 150 and 350 GeV/c^2 for the W' search and the M_{ee} cuts at 150 and 250 GeV/c^2 for the Z' search. Fig. 7 shows the plots for the higher mass cut. The obtained mass limits are $M_{W'} > 600$ GeV/c^2 and $M_{Z'} > 440$ GeV/c^2 at 95% CL.

9 B^0-$\overline{B}^0$ mixing

Although CDF and DØ detectors have been designed to pursuit high p_T physics, studies of b-physics are possible because of large b cross section of $\sim$10 μb ($p_T > 10$ GeV/c), which can be compared with 7 nb at LEP. The CDF silicon vertex detector can tag b decays, and is useful for the study of b production and decay.

B^0-$\overline{B}^0$ mixing emerges through the box diagrams in the Standard Model. Study of B^0-$\overline{B}^0$ mixing is particularly interesting if a time-dependent mixing in the B_s system is measured, from which the CKM matrix element V_{ts} can be derived. CDF has published the B^0-$\overline{B}^0$ mixing measurement in $e\mu$ channel[21] based on the 1988-89 data. Analysis using the 1992-93 data is in progress.

DØ reports the B^0-$\overline{B}^0$ mixing in dimuon channel. The mixing parameter χ is defined as: $\chi = prob(b \to \overline{B}^0 \to B^0 \to \ell^+ X)/prob(b \to \ell^{\pm} X)$. Since both B_d and B_s mesons are produced at the Tevatron energy, χ being measured is a mixture of these two states: $\chi = f_d\chi_d + f_s\chi_s$, where f_d and f_s are the fractions of the two states and χ_d and χ_s are the mixing probabilities in the B_d and B_s systems. The quantity measured by DØ is the like- to unlike-sign μ ratio: $[N(\ell^+\ell^+) + N(\ell^-\ell^-)]/N(\ell^+\ell^-)$. In addition to direct b and $\bar{b}$ decays, muons via c ($b \to c \to \mu$) and other processes contribute differently to the ratio. The following table shows the processes considered by DØ:

Type	like-sign	unlike-sign
$b \to \mu^-, \bar{b} \to \mu^+$	$2\chi(1-\chi)$	$(1-\chi)^2 + \chi^2$
$b \to \mu^-, \bar{b} \to \bar{c} \to \mu^-$	$(1-\chi)^2 + \chi^2$	$2\chi(1-\chi)$
$b \to c \to \mu^+, \bar{b} \to \bar{c} \to \mu^-$	$2\chi(1-\chi)$	$(1-\chi)^2 + \chi^2$
$b \to c\mu^-, c \to \mu^+$	0%	100%
$c \to \mu^+, \bar{c} \to \mu^-$	0%	100%
Drell-Yan, J/ψ , Υ	0%	100%
decay background	50%	50%

Contribution of each process is evaluated using a Monte Carlo simulation, and the derived mixing parameter is: $\chi = 0.13 \pm 0.02 \pm 0.05$. This measurement can be compared with

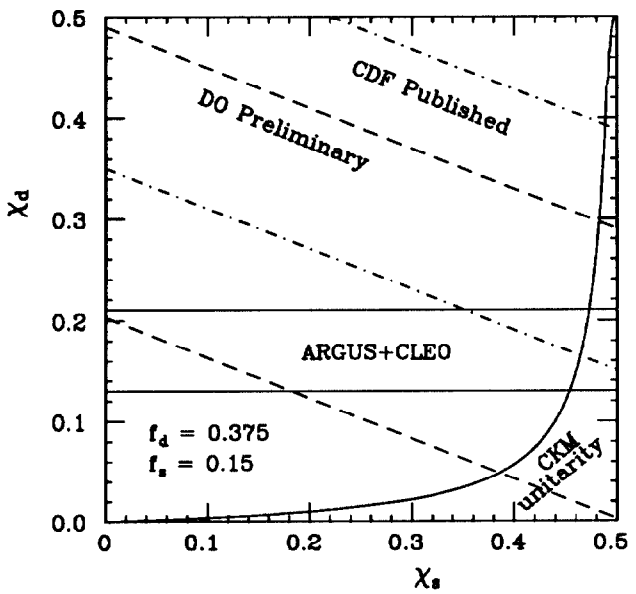

Figure 8: χ_d versus χ_s for CDF (dot-dashed) and DØ preliminary (dashed) values of χ. The lines indicate the 1-σ range of the uncertainty.

the published value by CDF: $\chi = 0.176 \pm 0.031(\text{stat} + \text{sys}) \pm 0.032(\text{model})$. The both measurements are shown in Fig. 8 in the $\chi_s - \chi_d$ plane. The fractions f_d and f_s are taken to be 0.375 and 0.15, respectively[22]. Also shown in the figure are measurements by ARGUS and CLEO[23], and the region allowed by CKM matrix unitarity. The results are consistent with full mixing in the B_s system.

10 B_u, B_d, B_s masses

The masses of B_u, B_d and B_s mesons are measured by CDF. Primarily, the large b cross section, excellent tracking ($\delta p_T / p_T \sim 0.0066 \oplus 0.0014 p_T$ [p_T in GeV/c]), and good muon identification allow to reconstruct the masses in the fully exclusive decay channels with remarkable clarity.

The B meson masses are reconstructed in the exclusive decay modes:

- $B_u \to J/\psi K^+$ with $J/\psi \to \mu^+\mu^-$
- $B_d \to J/\psi K^{*0}$ with $J/\psi \to \mu^+\mu^-$ and $K^{*0} \to K^+\pi^-$
- $B_s \to J/\psi\phi$ with $J/\psi \to \mu^+\mu^-$ and $\phi \to K^+K^-$

and in their charge conjugate modes. Reconstruction of B_s's, for example, requires a dimuon consistent with a J/ψ and two oppositely charged tracks whose invariant mass consistent with a ϕ when their masses are assumed to be of K. The dimuon and (K^+K^-) invariant mass distributions are shown in Fig. 9. Events are retained if the dimuon mass agrees with J/ψ within 100 MeV, and the K^+K^- mass with ϕ within 10 MeV. In addition, the

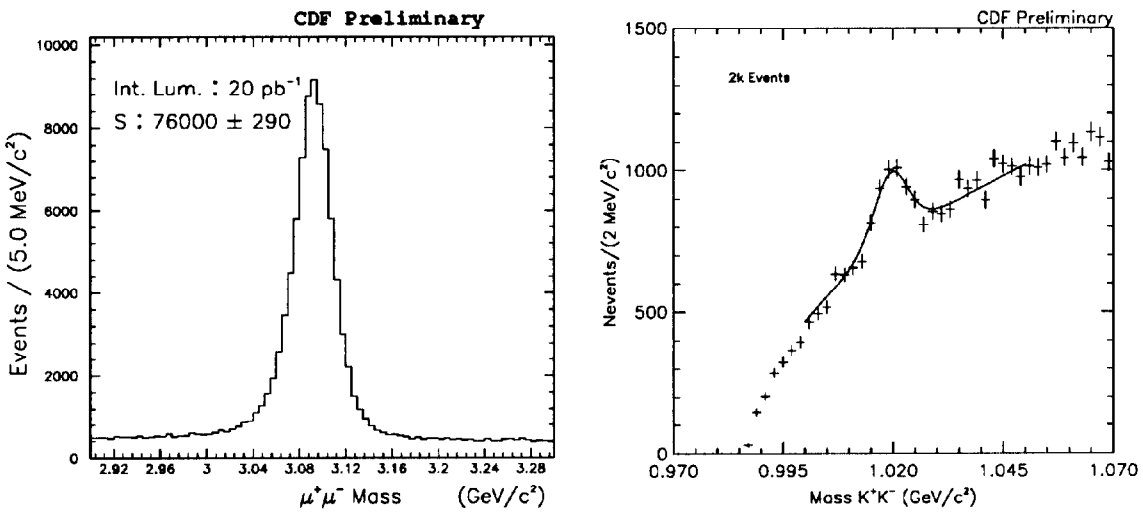

Figure 9: Dimuon and (K^+K^-) invariant mass distributions.

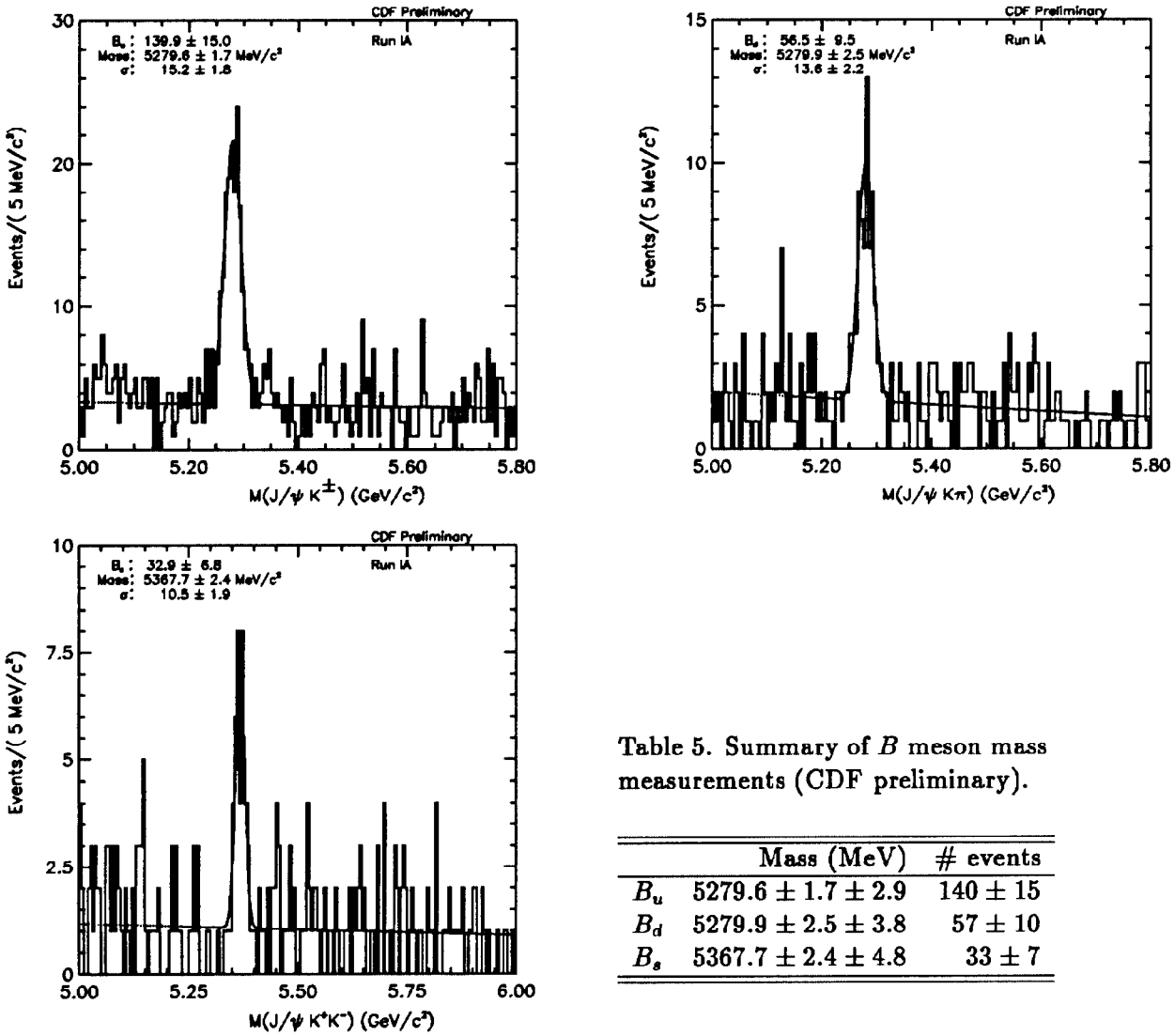

Table 5. Summary of B meson mass measurements (CDF preliminary).

	Mass (MeV)	# events
B_u	$5279.6 \pm 1.7 \pm 2.9$	140 ± 15
B_d	$5279.9 \pm 2.5 \pm 3.8$	57 ± 10
B_s	$5367.7 \pm 2.4 \pm 4.8$	33 ± 7

Figure 10: B meson masses reconstructed in the exclusive decay modes.

reconstructed B is required that $p_T > 6$ GeV/c, $c\tau$ measured with SVX/CTC is positive, and B points back to the primary vertex with CL(χ^2)>1%.

The reconstructed B_s mass distribution is shown in Fig. 10, together with B_u and B_d mass distributions. The peak is fit to a Gaussian plus a linear background. The lower mass range is excluded in the fit since it can include contributions from higher multiplicity B decays. The fitted mass values and the numbers of signals in 21 pb^{-1} are summarized in Table 5. The systematic uncertainty includes effects of mass fitting, selection criteria, momentum scale uncertainty, and detector alignment. The B_s mass measurements by CDF and the LEP experiments[24] are compared in Fig. 11. CDF measures the mass with a smallest uncertainty.

The world average $(D_s - D)$ mass difference is 99.5 ± 0.6 MeV[25]. Assumption that the $SU(3)$ flavor splitting in the B system has the same magnitude as in the D system predicts

the B_s mass in the range indicated by box in Fig. 11. Although there is a tendency that the B_s mass measured is slightly smaller than the prediction, the CDF data is consistent within the uncertainty.

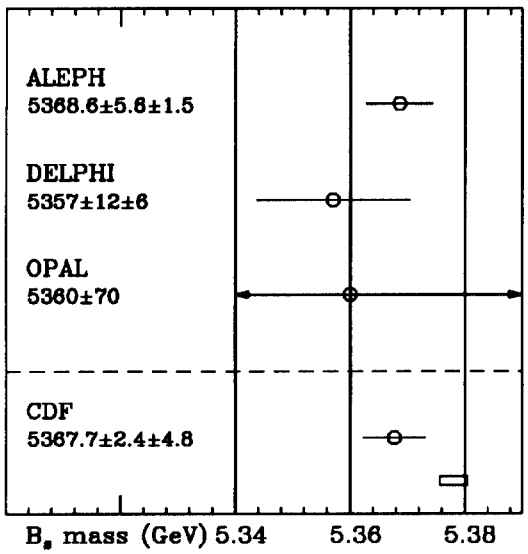

Figure 11: Comparison of B_s mass measurements by CDF and LEP experiments. The mass is measured using the $J/\psi\ \phi$ decay mode (DELPHI, OPAL and CDF), $\psi'\phi$ decay mode (ALEPH) and semileptonic decay mode D_sX (ALEPH and DELPHI). $m_B + |m_{D_s} - m_D|$ taken from PDG is shown (open box) as comparison.

11 B_u, B_d, B_s lifetimes

Measurement of B meson lifetimes is particularly important to understand the hierarchy of B meson lifetimes. Some models predict that $\tau^+ > \tau_{B_s} > \tau^0 > \tau_{\Lambda_b}$ but they agree to within 10%–20%. Silicon vertex detector is extensively used to measure the lifetimes. The strip dimension of SVX is 60 μm wide in ϕ and 85 cm long in z. There are six strips aligned along z. There are four layers arranged along the particle trajectory in the range r = 3 cm to 7.9 cm. The impact point resolution is evaluated to $\sigma_D(p_T) = 8 \oplus 45/p_T$ (μm).

The lifetimes of B_u and B_d are measured by the exclusive decays: $B \to J/\psi\ K$. The proper decay length is calculated from the decay point measured with SVX. The proper decay length distributions for charged and neutral B's, for both the signal and sideband regions are shown in Fig. 12.

The signal region is defined to be within $\pm$30 MeV of the world average B mass[25], and the sideband regions to be between 60 and 120 MeV away from the world average. The signal is parameterized as an exponential convoluted with a Gaussian resolution function, while the background parameterized as a Gaussian plus asymmetric exponential tails. The signal and sideband distributions are fit simultaneously.

The B_s lifetime is measured from partially reconstructed $\ell + D_s$; $B_s \to D_s^+ \ell^- X$ with subsequent $D_s^+ \to \phi\pi$ and $\phi \to K^+K^-$ decays. Since the transverse momentum of the B_s can not be measured directly, CDF defines:

$$c\tau = \frac{L_B M_B}{p_T(B)} = \frac{L_B M_B}{p_T(D_s\ell^-)} \cdot \frac{p_T(D_s\ell^-)}{p_T(B)} \equiv c\tau^* \cdot K, \tag{6}$$

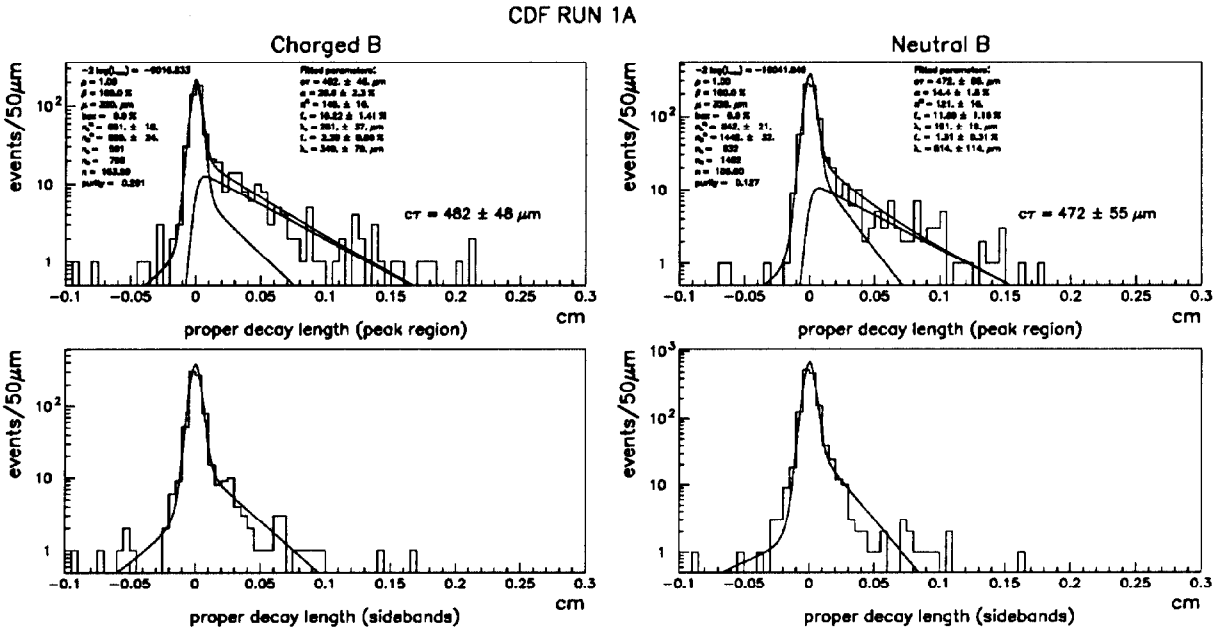

Figure 12: B_u and B_d proper time distributions.

where L_B is the transverse decay length of the B and $p_T(D_s\ell^-)$ is the transverse momentum of the $D_s+\ell^-$ system. The partially corrected decay length, $c\tau^*$, is quantity directly measurable and the correction factor, K, is determined using a Monte Carlo simulation.

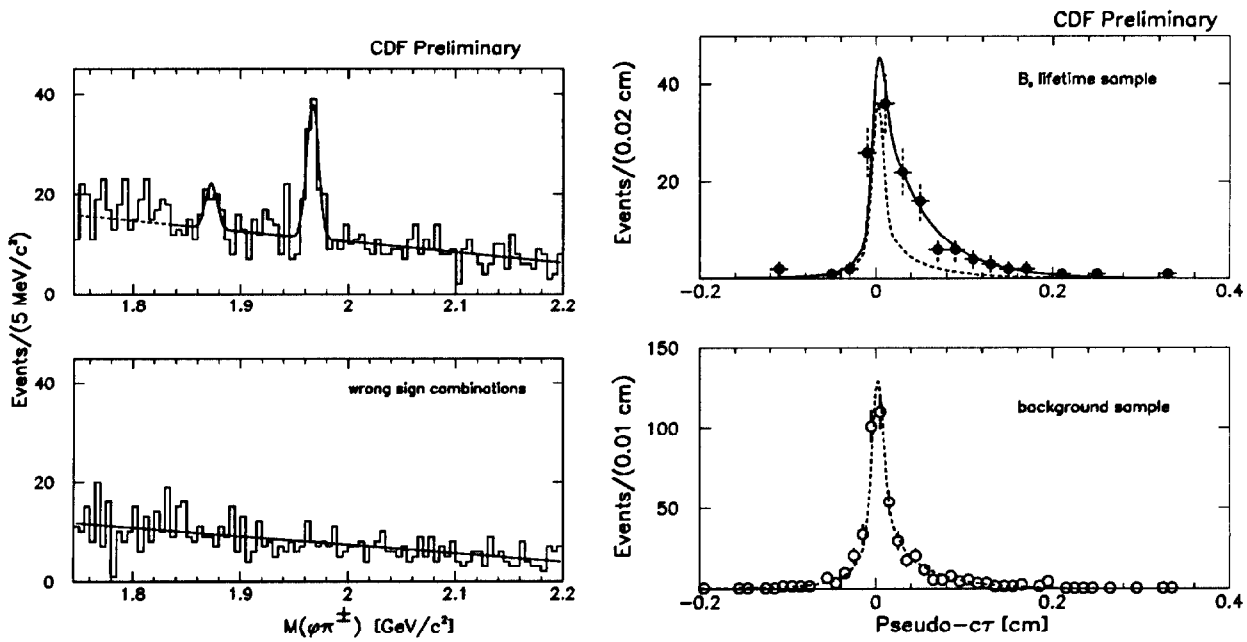

Figure 13: $\phi\pi^+$ mass distribution, showing a D_s^+ signal in the right sign data. $c\tau^*$ distributions of the signal and background regions.

Fig. 13 shows the $\phi\pi^+$ invariant mass distributions and the pseudo-$c\tau$ ($c\tau^*$) distributions for the signal and background regions. A D_s^+ peak can be seen in the right sign data in which oppositely charged lepton is reconstructed. The peak at 1.87 GeV/c^2 corresponds to D^+ from $\overline{B}^0$ decay. No peak is seen in the wrong sign data. The signal sample contains a combinatorial background under the D_s mass peak. In order to extract a lifetime from the observed $c\tau^*$ distribution, the D_s sidebands (excluding D region) in the right sign $\phi\pi$ mass spectrum and the wrong sign combinations are used to get the $c\tau^*$ distribution of the background.

The CDF preliminary lifetime measurement of B mesons is summarized and compared with LEP measurements[24] in Fig. 14. The CDF measurement of the ratio, τ^+/τ^0, is $1.02 \pm 0.16 \pm 0.05$, which can be compared with the corresponding value 2.5 in the D system.

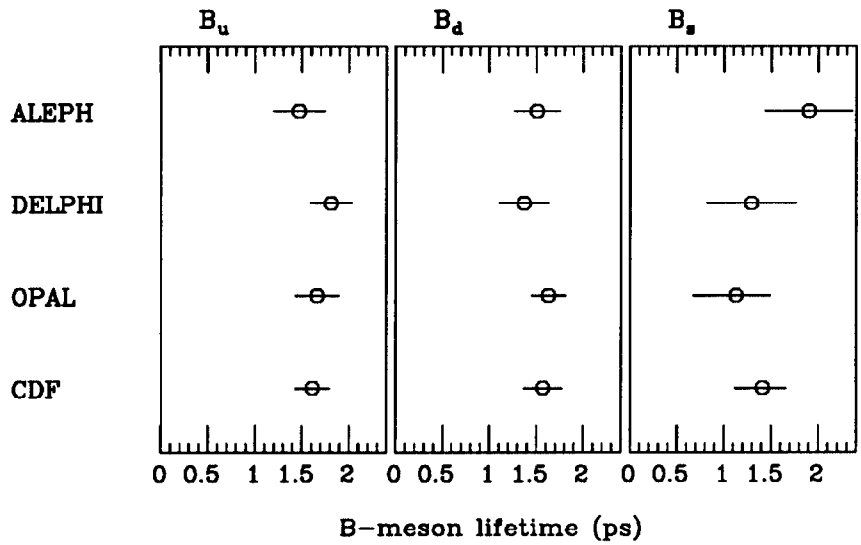

Figure 14: Comparison of B-meson lifetime measurements.

12 Summary

The Tevatron Collider at Fermilab is providing wide variety of interesting physics opportunities.

Precise measurements of the Standard Model parameters such as the W mass and the width are unique with the Tevatron. Tests of the Standard Model include the measurements of trilinear boson couplings through the reactions $W\gamma$, $Z\gamma$, $W + Z$ at present, and others in near future. The proton structure functions are being illuminated through W and Z decay asymmetry measurements. Physics beyond the Standard Model is searched for from W' and Z'.

CDF is capable of pursuing detailed study of b in terms of B hadron spectroscopy and lifetime measurements. The study is expected to extended to cover the time-dependent B^0-$\overline{B}^0$ mixing and CP violation.

13 Acknowledgements

I would like to thank the CDF and DØ electroweak and b-physics coordinators, L. Nodulman, M. Demarteau, F. DeJongh for providing me with the updated data, and all the members who worked hard to collect and analyze the data. Discussions with N. Oshima on the DØ data were helpful. I wish to thank many authors of the proceedings of "9th topical workshop on proton-antiproton physics", Tsukuba, Oct. 1993, which helped me to outline the present talk.

References

[1] F. Abe *et al.* (CDF collaboration), Nucl. Instr. and Methods, A271, 387 (1988).

[2] S. Abachi *et al.* (DØ collaboration), Nucl. Instr. and Methods A338, 185 (1994).

[3] M. Swartz, "High energy tests of the electroweak standard model", 1993 International Symposium on Lepton-Photon Interactions at High Energies.

[4] P. Arnold and R.P. Kauffman, "W and Z production at next-to-leading order: from large q_T to small", ANL-HEP-PR-90-70.

[5] A.D. Martin, R.G. Roberts, W.J. Stirling, Phys. Lett. 228B, 149 (1989).

[6] S. Lami and D. Wood, DØ note #1462, 1992 (unpublished); the systematic error includes the effects of different structure functions.

[7] J. Rosner, W. Worah, T. Takeuchi, Enrico Fermi Institute Preprint, EFI-93-40 (1993).

[8] The LEP collaborations and the LEP Electroweak Working Group, Europhysics Conference on High Energy Physics, Marseille, 1993; and 1993 International Symposium on Lepton-Photon Interactions at High Energies, Cornell.

[9] The LEP collaborations: ALEPH, DELPHI, L3 and OPAL, Phys. Lett. B276, 247 (1992).

[10] F. Abe *et al.* (CDF collaboration), Phys. Rev. Lett. 69, 28 (1992).

[11] R. Hamberg, W.L. Van Neerven and Matsuura, Nucl. Phys. B359, 343 (1991).

[12] F. Abe *et al.* (CDF collaboration), Fermilab PUB-94/051-E, submitted to Phys. Rev. Lett.

[13] U. Baur and D. Zeppenfeld, Phys. Lett. B201, 383 (1988).

[14] J. Alitti *et al.* (UA2 collaboration), Phys. Lett. B277, 194 (1992).

[15] K. Hagiwara *et al.*, Nucl. Phys. B282, 253 (1987).

[16] U. Baur and E.L. Berger, Phys. Rev. D41, 1476 (1990); U. Baur and E.L. Berger, FSU-HEP-921030.

[17] Similar assumptions have been made by CDF for $W\gamma$ anomalies, where $n = 2$ and $\Lambda = 1.5$ TeV are assumed. These assumptions, however, do not change much the final results for $W\gamma$. The assumptions for $Z\gamma$ assure that the high energy behavior of the terms proportional to $h_{1,3}$ is the same as $h_{2,4}$ and that the present anomalies do not violate unitarity. The limits on the anomalies are dependent on the assumptions to a $\sim$ 10% level.

[18] A.D. Martin, R.G. Roberts, W.J. Stirling, Mod. Phys. Lett. A4, 1135 (1989).

[19] F. Abe *et al.* (CDF collaboration), Phys. Rev. Lett. 67, 2609 (1991); F. Abe *et al.* (CDF collaboration), Phys. Rev. Lett. 68, 1463 (1992).

[20] K. Maeshima, Proceedings for 9th Topical Workshop on Proton-antiproton Collider Physics, Tsukuba, Oct. 1993.

[21] F. Abe *et al.* (CDF collaboration), Phys. Rev. Lett. 67, 3351 (1991).

[22] H. Adeva *et al.* (LEP collaboration), Phys. Lett. B200, 221 (1990); D. Decamp *et al.* (MARK II collaboration), Phys. Lett. B258, 236 (1991); H.C. Albajar *et al.* (UA1 collaboration), Phys. Lett. B262, 171 (1991).

[23] H. Albrecht *et al.* (ARGUS collaboration), Phys. Lett. B192, 245 (1987); M. Artuso *et al.* (CLEO collaboration), Phys. Rev. Lett. 62, 2233 (1989).

[24] The data are presented at various conferences in 1993; See also S. Squarcia, "Heavy flavour physics at LEP", these proceedings.

[25] K. Hikasa *et al.* (Particle data Group), Phys. Rev. D45, 1 (1992).